Seasonal Impact of Adjacency Effects on Ocean Color Radiometry at the AAOT Validation Site

Barbara Bulgarelli and Giuseppe Zibordi

***Abstract*— The seasonal impact of adjacency effects (AE) on satellite ocean color data at visible and near-infrared (NIR) wavelengths by the Sea-Viewing Wide Field-of-View Sensor, the Moderate Resolution Imaging Spectroradiometer onboard the Aqua platform (MODISA), the Medium Resolution Imaging Spectrometer, the Ocean and Land Color Instrument, the Operational Land Imager (OLI), and the MultiSpectral Imagery (MSI) was theoretically evaluated at a validation site in the northern Adriatic Sea. The analysis made use of comprehensive simulations accounting for multiple scattering, sea surface roughness, sensor viewing geometry, actual coastline, typical and extreme atmospheric conditions, and the seasonal variability of solar illumination and, land and water optical properties. Results, obtained by relying on the normalization of the radiometric sensitivity of each sensor to the same input radiance, show that the spectral and seasonal impacts of AE considerably vary among sensors. AE significantly exceed the radiometric sensitivity of MSI at its sole blue band in winter, whereas they significantly outdo the noise threshold of OLI and MODISA high-resolution data exclusively in the NIR in summer. Conversely, for all other sensors and for MODISA low-resolution data, AE are particularly significant at NIR bands between March and October and at the blue–green bands in winter.**

***Index Terms*— Adjacency effects (AE), ocean colors, optical remote sensing.**

I. Introduction

STANDARD algorithms for the processing of ocean color satellite data usually assume an infinite water surface. Because of this, the presence of the nearby land is neglected in coastal waters. Consequently, the radiance reflected by the land and then scattered by the atmosphere into the sensor field-of-view becomes a source of perturbations leading to uncertainties in ocean color radiometric data. These perturbations are called *adjacency effects* (AE), and the related spectral difference in the top-of-atmosphere radiance between the case accounting for the nonuniformity of the underlying surface and the case assuming a uniform surface is named *adjacency radiance* L_{adj}. The sign of L_{adj} can hence be both positive and negative.

A comprehensive analysis of AE in ocean color remote sensing of coastal waters was recently performed at the Sea-Viewing Wide Field-of-View Sensor (SeaWiFS)-equivalent center wavelengths for most relevant ocean color sensors and a wide range of mid-latitude coastal environments [1]. Typical observation conditions by the SeaWiFS, the Moderate Resolution Imaging Spectroradiometer onboard the Aqua platform (MODISA), the Medium Resolution Imaging Spectrometer (MERIS), the Ocean and Land Color Instrument (OLCI), the Operational Land Imager (OLI), and the MultiSpectral Imagery (MSI) sensors were considered. Importantly, in view to standardize the analysis, the signal-to-noise ratio (SNR) of each sensor was normalized to the same input radiance.

The results showed that AE in radiometry data from the less sensitive SeaWiFS, OLI, and MSI, as well as from MERIS and OLCI in full spatial resolution (FR), are still above the sensor radiometric sensitivity at 36 km offshore (20 km for MSI) and at all wavelengths for highly reflecting land covers (e.g., snow, dry vegetation, white sand, and concrete). Conversely, for land covers characterized by vegetation or bare soil, AE at visible wavelengths may become lower than the sensor radiometric sensitivity at a closer distance from the coast. Such a distance increases with the radiometric resolution of the sensor. The more sensitive MERIS and OLCI reduced spatial resolution (RR) data together with MODISA low-resolution (LR) data indicate that AE still exceed the sensor noise threshold at 36 km offshore for all land covers and at all SeaWiFS-equivalent center wavelengths, excluding the red for land covers characterized by green vegetation.

Considering the previous sensors and the additional MODISA high resolution (HR), this letter presents a detailed analysis of the seasonal impact of AE in satellite radiometry data at the Aqua Alta Oceanographic Tower (AAOT, 45.31°N, 12.51°E) site located in the northern Adriatic Sea at about 8 nmi from the coast. It is mentioned that the AAOT, which is included in the Ocean Color component of the Aerosol Robotic Network (AERONET-OC) [2], is a recognized site for the validation of ocean color products [3].

The analysis relies on realistic simulations of AE performed accounting for a comprehensive characterization of the regional intra-annual optical properties of atmosphere and water, as derived from a multiannual time series of *in situ* measurements [3], [4]. The simulated data embrace average and extreme atmospheric conditions, seasonal land and sea optical properties and illumination geometries, and account for the actual coastline [5], [6].

A detailed picture of the intra-annual impact of AE in satellite data at the AAOT by the most used ocean color sensors is regarded as relevant for validation and eventually vicarious calibration of satellite data. With this respect, the AAOT site is currently considered for the vicarious calibration of MSI.

Manuscript received August 4, 2017; revised December 4, 2017; accepted December 6, 2017. Date of publication February 23, 2018; date of current version March 23, 2018. *(Corresponding author: Barbara Bulgarelli.)*

The authors are with the Joint Research Centre of the European Commission, 21027 Ispra, Italy (e-mail: barbara.bulgarelli@ec.europa.eu; giuseppe.zibordi@ec.europa.eu).

Color versions of one or more of the figures in this letter are available online at http://ieeexplore.ieee.org.

Digital Object Identifier 10.1109/LGRS.2017.2781900

TABLE I

PARAMETERS DEFINING THE ILLUMINATION AND OBSERVATION GEOMETRIES ADOPTED IN THE SIMULATIONS (AFTER [1])

θ_0	25^o - 45^o - 65^o	
θ_v	5^o [MER,MODA,OLCI,MSI,OLI] 20^o [MER,MODA,SWF,OLCI,MSI] 50^o [MODA,SWF,OLCI]	
ϕ_0	-160^o	$+160^o$
ϕ_v	-100^o [SWF,MODA] $+75^o$[MODA]	-75^o[MER,OLCI,MSI,OLI] $+100^o$[MER, SWF,OLCI,MSI,OLI]

SWF=SeaWiFS, MER=MERIS, MODA=MODISA. Positive and negative satellite azimuths (counted clock-wise from the north direction) indicate observations from over the sea, and from over the land, respectively.

II. METHODS AND BACKGROUND

Intra-annual AE, quantified through the simulated at-sensor adjacency radiance L_{adj}, are analyzed with respect to the standardized radiometric sensitivity of the various sensors, expressed in terms of the Noise Equivalent Radiance Difference $NE\Delta L$. At each wavelength, $NE\Delta L$ defines the at-sensor incremental radiance that can still be discriminated from noise when observing a typical signal [7]. Notably, $NE\Delta L$ is often set equivalent to one digital number to maximize sensor performance. In this analysis, any adjacency radiance contribution lower than $NE\Delta L$ is considered not detectable.

A. Simulation Procedure

As already anticipated, simulations of L_{adj} were performed at SeaWiFS-equivalent center wavelengths ($\lambda = 412$, 443, 490, 510, 555, 670, 765, and 865 nm) adopting the methodology proposed by Bulgarelli *et al.* [5] by applying the 3-D Novel Adjacency Perturbation Simulator for Coastal Area Monte Carlo code [5] and the finite-element (FEM) plane-parallel numerical code [8]–[10].

1) Illumination and Observation Geometries: Illumination and observation geometries typical of the AAOT site are given in Table I [1], [5] for the various sensors. Specifically, θ_0 and ϕ_0 represent the solar zenith and azimuth angles, respectively, while θ_v and ϕ_v indicate the viewing angle and the satellite azimuth, respectively. The solar zenith angle θ_0 was set to 25° and 65° for typical May–August and November–February observations, respectively, and to 45° in all other cases.

2) Atmospheric Optical Properties: Seasonal atmospheric cases were determined by different values of the Ångström coefficient (i.e., $\alpha = 0.02$, 0.05, and 0.08) and exponent (i.e., $\nu = 1.4$, 1.7, and 1.9) assuming an aerosol scale height $H_a = 1.2$ km.

3) Land Optical Properties: Intra-annual land spectral albedos ρ_l were determined as

$$\rho_l = (1 - S_E) \cdot \langle \text{DHR} \rangle + S_E \cdot \langle \text{BHR}_{\text{iso}} \rangle \quad (1)$$

where S_E indicates the diffuse-to-direct irradiance ratio at the surface, DHR indicates the directional hemispherical reflectance, and BHR_{iso} indicates the isotropic bihemispherical reflectance [11]. The values of $\langle \text{DHR} \rangle$ and $\langle \text{BHR}_{\text{iso}} \rangle$ were inferred from spatially averaged MODIS-HR multiannual climatological reflectance products [12] assuming a cropland albedo [5]. Values of the intra-annual spectral land albedos are illustrated in Fig. 1(a) for $\theta_0 = 45°$, $\alpha = 0.05$, and $\nu = 1.7$.

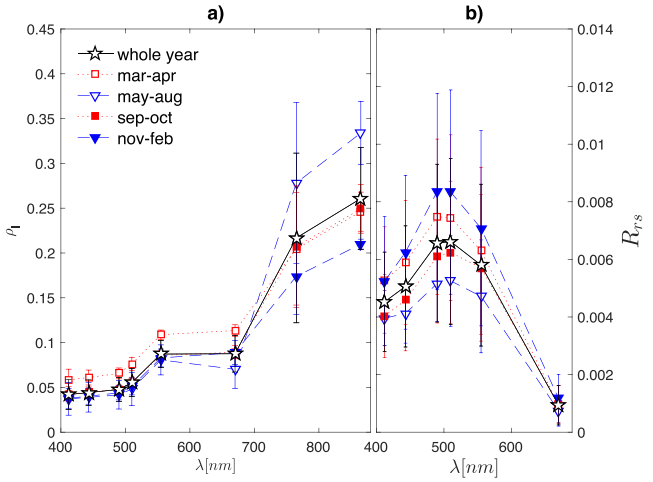

Fig. 1. Spectral values of (a) time and spatially averaged land albedo ρ_l for $\theta_0 = 45°$, $\alpha = 0.05$, and $\nu = 1.7$, and (b) *in situ* R_{rs} [sr^{-1}] adopted in the simulations. Symbols represent different annual and intra-annual periods. Error bars indicate the standard deviation.

4) Water Optical Properties: The AAOT time series of *in situ* measurements [3], [13] was used to define intra-annual values of the remote sensing reflectance R_{rs} [Fig. 1(b)]. Conversely, the values of R_{rs} in the near-infrared (NIR) were assumed null in agreement with a negligible sensitivity of AE to non-null NIR water signals at the AAOT [6]. Wind speed, relevant to determine the reflectance properties of the water surface, was set to $w = 1$, 3.3, and 6 ms^{-1}.

B. Standardized Sensors' Radiometric Sensitivity

For each sensor, the average values of the SNR [1], [14] normalized to the same input radiance L_{typ} typical of cloud-free ocean data acquisitions at $\theta_0 = 45°$ were considered applicable to spring and fall data, too. Conversely, SNR values for summer and winter data were determined by adjusting the on-orbit values to L_{typ} at $\theta_0 = 30°$ and 70° [14], respectively. Corresponding values of $NE\Delta L$ were obtained as $NE\Delta L = L_{\text{typ}}/\text{SNR}$.

III. RESULTS AND DISCUSSION

For each satellite sensor, Fig. 2 shows values of the mean adjacency radiance $\bar{L}_{\text{adj}}$ at the AAOT obtained by averaging L_{adj} over the observation conditions detailed in Table I. One and two sensor $NE\Delta L$ are also displayed. Values of $\bar{L}_{\text{adj}}$ are slightly larger for SeaWiFS that performs off-nadir observations, and slightly lower for OLI that conversely only does nadir observations. The results show that:

1) For MODIS-HR, MSI, and OLI, average AE are always very close to noise.

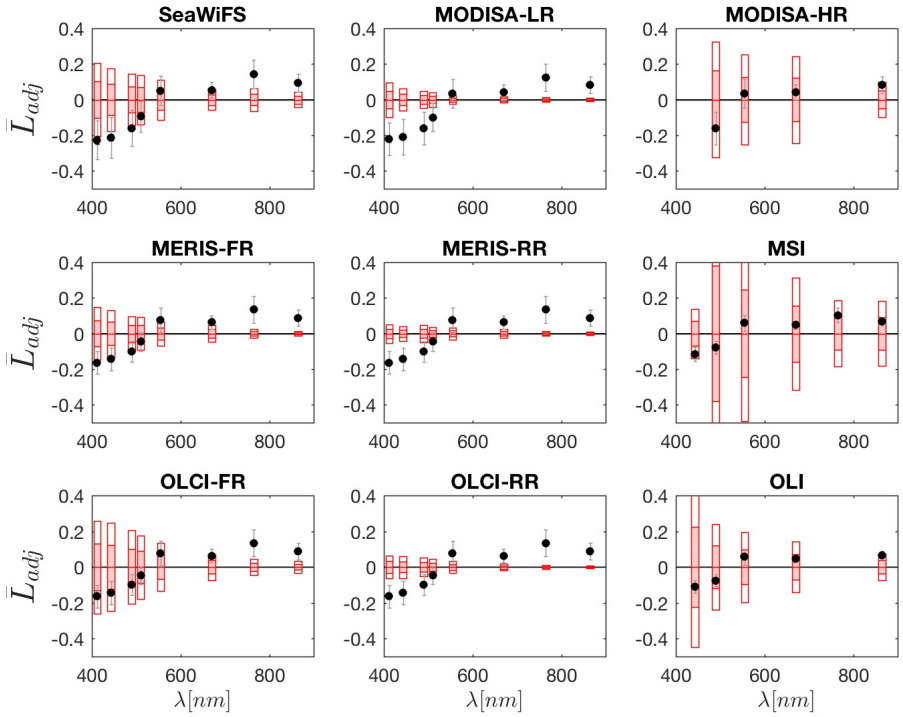

Fig. 2. Spectral annual average values of $\bar{L}_{\text{adj}}$ [$\text{W} \cdot \text{m}^{-2} \cdot \mu\text{m}^{-1} \cdot \text{sr}^{-1}$] at SeaWiFS-equivalent center wavelengths for the various sensors. Black error bars represent uncertainties computed assuming uncorrelated contributions; gray error bars indicate ± 1 standard deviation ($N = 6$ for OLI, $N = 12$ for MSI, $N = 18$ for the other sensors). Shaded and empty box bars indicate one and two harmonized sensor spectral $NE\Delta L$, respectively.

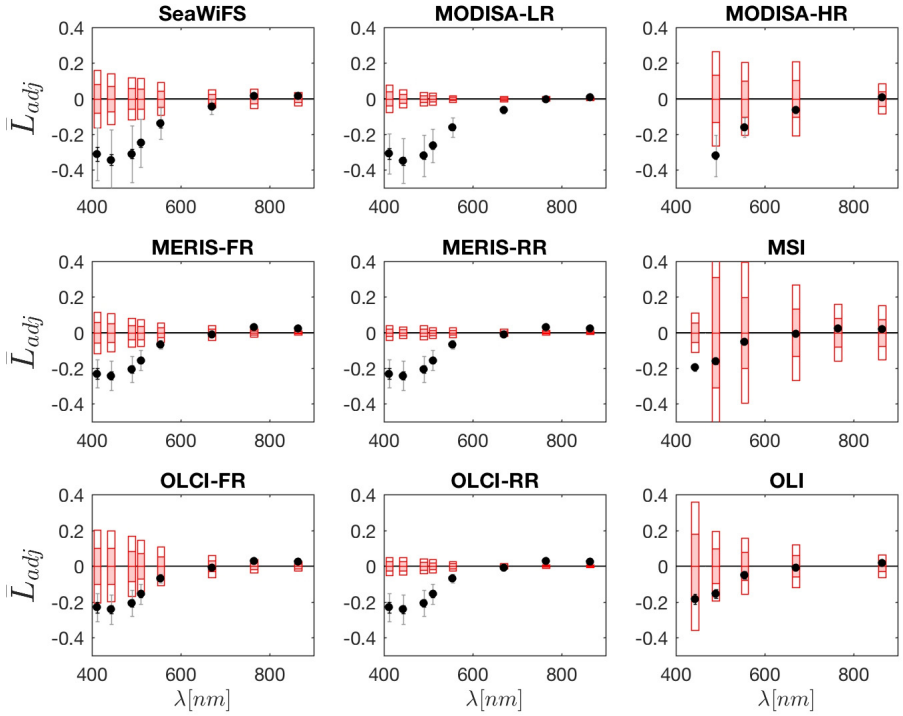

Fig. 3. Values of $\bar{L}_{\text{adj}}$ [$\text{W} \cdot \text{m}^{-2} \cdot \mu\text{m}^{-1} \cdot \text{sr}^{-1}$] for the November–February period at SeaWiFS-equivalent center wavelengths for the various sensors. Black error bars represent uncertainties computed assuming uncorrelated contributions; gray error bars indicate ± 1 standard deviation ($N = 2$ for OLI, $N = 4$ for MSI, $N = 6$ for the other sensors). Shaded and empty box bars indicate one and two harmonized sensor spectral $NE\Delta L$, respectively.

2) For SeaWiFS, MERIS-FR, and OLCI-FR, annual $\bar{L}_{\text{adj}}$ values are very close to noise in the visible, while they significantly exceed $NE\Delta L$ in the NIR.
3) For the more sensitive MODISA-LR, MERIS-RR, and OLCI-RR, annual average adjacency perturbations significantly exceed the noise at both blue and NIR wavelengths.

Although AE at the AAOT vary with the sensor viewing angle and the atmospheric turbidity (as detailed in Bulgarelli *et al.* [5]), their detectability does not show

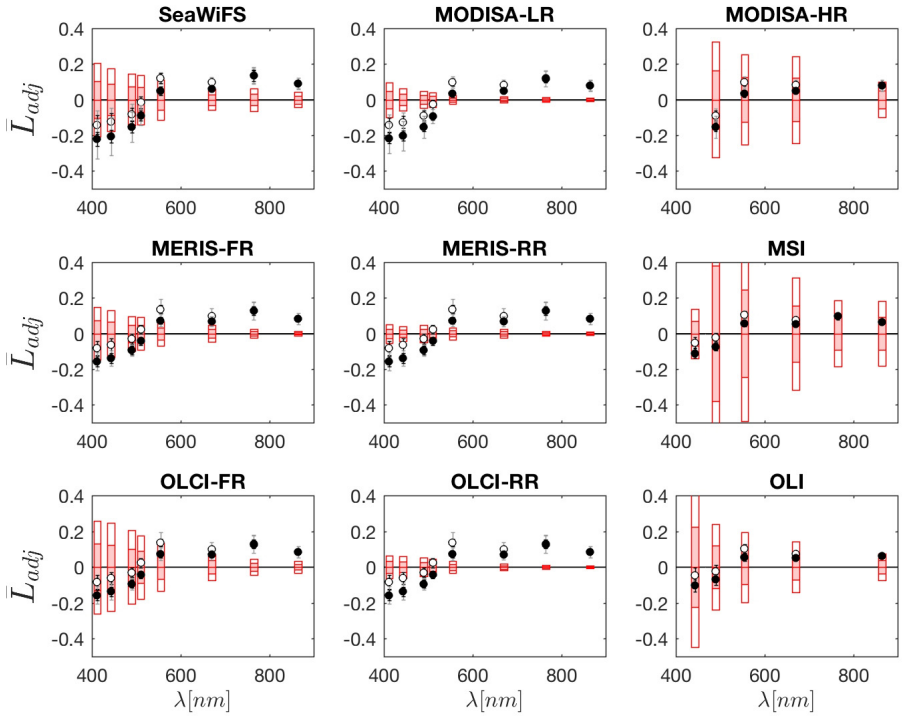

Fig. 4. Values of $\bar{L}_{\mathrm{adj}}$ [$\mathrm{W \cdot m^{-2} \cdot \mu m^{-1} \cdot sr^{-1}}$] for the sole periods of March–April (empty circles) and September–October (filled circles) at SeaWiFS-equivalent center wavelengths for the various sensors. Black error bars represent uncertainties computed assuming uncorrelated contributions; gray error bars indicate ± 1 standard deviation ($N = 2$ for OLI, $N = 4$ for MSI, $N = 6$ for the other sensors). Shaded and empty box bars indicate one and two harmonized sensor spectral $NE\Delta L$, respectively.

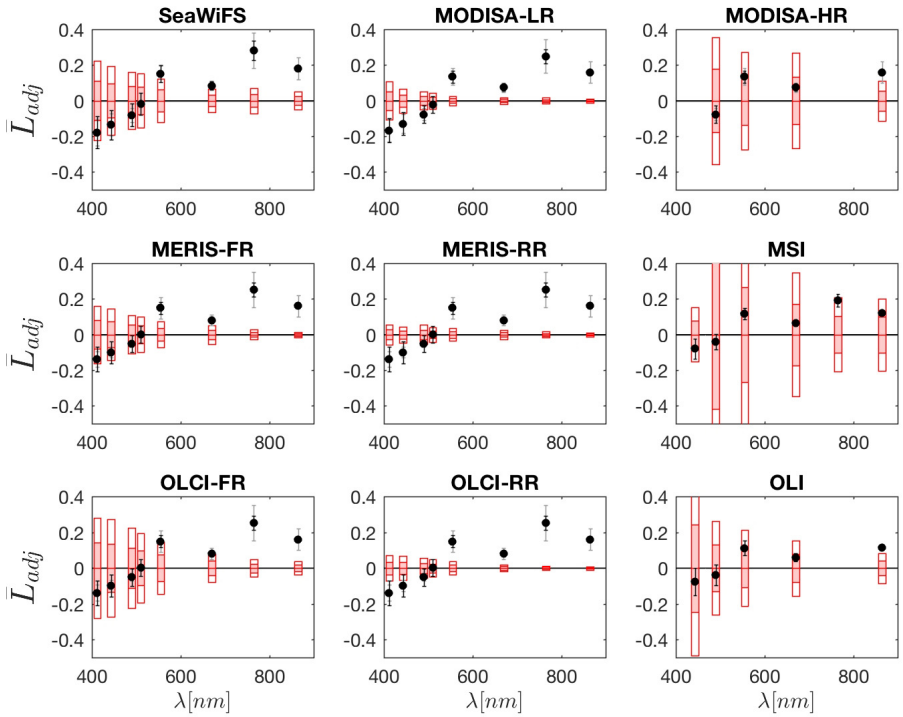

Fig. 5. Values of $\bar{L}_{\mathrm{adj}}$ [$\mathrm{W \cdot m^{-2} \cdot \mu m^{-1} \cdot sr^{-1}}$] for the May–August period at SeaWiFS-equivalent center wavelengths for various sensors. Black error bars represent uncertainties computed assuming uncorrelated contributions; gray error bars indicate ± 1 standard deviation ($N = 2$ for OLI, $N = 4$ for MSI, $N = 6$ for the other sensors). Shaded and empty box bars indicate one and two harmonized sensor spectral $NE\Delta L$, respectively.

sensitivity to these parameters. Conversely, the detectability of AE has a significant intra-annual variation (see Figs. 2–5).

AE are always close or below the noise threshold of MODIS-HR, MSI and OLI data, apart from summer data in the NIR by OLI and MODIS-HR and, winter data in the blue by MSI. SeaWiFS and MERIS-FR data are significantly affected by AE at the NIR wavelengths between March and October and at the blue wavelengths

in winter. Conversely, AE are detectable in sole OLCI-FR NIR data between March and October. For MODISA-LR, MERIS-RR, and OLCI-RR, the adjacency radiance significantly exceeds $NE\Delta L$ in the blue–green bands between September and February, in red and NIR bands from March to October, and at the additional yellow bands in summer. It is, however, recognized that the confidence on simulated adjacency perturbations in winter and at visible wavelengths is lower [5].

IV. Conclusion

The seasonal impact of AE on SeaWiFS, MODISA, MERIS, OLCI, OLI, and MSI data acquired at the AAOT site was theoretically investigated at SeaWiFS-equivalent center wavelengths under typical observation conditions accounting for standardized average and intra-annual values of the SNR.

The results show that the seasonal and spectral impacts of AE on satellite radiometry data at the AAOT vary among the considered sensors. Nonetheless, a common trend can be individuated, evidencing summer AE very close to noise at the visible wavelengths and exceeding the noise level in the NIR, while the opposite occurs in winter. It is yet worthwhile mentioning that winter simulations at the visible wavelengths might highly depend on actual wind speed and direction, as well as on the actual mutual position of land, sun, and sensor, so that larger uncertainties are expected.

The seasonal variability of the impact of AE contributes to explaining observed intra-annual trends in biases of radiometric products from SeaWiFS and MODISA-LR data acquired at the AAOT between 2002 and 2010, which indeed showed significant negative departures from average biases at the red wavelengths in summer and consistent positive departures at the blue and red wavelengths in winter [15]. The high sensitivity of MODISA-LR to adjacency perturbations further explains the larger departures observed in MODISA-LR data with respect to SeaWiFS ones.

The results highlight the need to identify and eventually quantify AE for any sensor utilized for validation and/or vicarious calibration of ocean color data, while they further suggest taking advantage of the seasonality in the detectability of AE when performing exercises of validation and vicarious calibration.

Acknowledgment

The authors would like to thank Dr. Z. Szantoi for his valuable suggestions.

References

[1] B. Bulgarelli and G. Zibordi, "A cross-comparison of adjacency effects in SeaWiFS, MODIS-A, MERIS, OLCI, OLI and MSI observations," *Remote Sens. Environ.*, 2018.

[2] G. Zibordi *et al.*, "AERONET-OC: A network for the validation of ocean color primary products," *J. Atmos. Ocean. Technol.*, vol. 26, no. 8, pp. 1634–1651, 2009.

[3] J. F. Berthon, G. Zibordi, J. P. Doyle, S. Grossi, D. van der Linde, and C. Targa, "Coastal atmosphere and sea time series (CoASTS), Part 2: Data analysis," NASA GSFC, Greenbelt, MD, USA, Tech. Rep. 2002-206892, 2002, vol. 20, pp. 1–25.

[4] J.-F. Berthon, F. Mélin, and G. Zibordi, "Ocean colour remote sensing of the optically complex european seas," in *Remote Sensing of the European Seas*, V. Baraleand M. Gade, Eds. Dordrecht, The Netherlands: Springer, 2008.

[5] B. Bulgarelli, V. Kiselev, and G. Zibordi, "Simulation and analysis of adjacency effects in coastal waters: A case study," *Appl. Opt.*, vol. 53, no. 8, pp. 1523–1545, 2014.

[6] B. Bulgarelli, V. Kiselev, and G. Zibordi, "Adjacency effects in satellite radiometric products from coastal waters: A theoretical analysis for the northern Adriatic Sea," *Appl. Opt.*, vol. 56, no. 4, pp. 854–869, 2017.

[7] I. S. Robinson, *Measuring the Oceans From Space*. Springer-Verlag, 2004.

[8] B. Bulgarelli, V. Kisselev, and L. Roberti, "Radiative transfer in the atmosphere–ocean system: The finite-element method," *Appl. Opt.*, vol. 38, no. 9, pp. 1530–1542, 1999.

[9] B. Bulgarelli and J. P. Doyle, "Comparison between numerical models for radiative transfer simulation in the atmosphere–ocean system," *J. Quant. Spectrosc. Radiat. Transf.*, vol. 86, no. 3, pp. 315–334, 2004.

[10] B. Bulgarelli, G. Zibordi, and J.-F. Berthon, "Measured and modeled radiometric quantities in coastal waters: Toward a closure," *Appl. Opt.*, vol. 42, no. 27, pp. 5365–5381, 2003.

[11] J. V. Martonchik, C. J. Bruegge, and A. H. Strahler, "A review of reflectance nomenclature used in remote sensing," *Remote Sens. Rev.*, vol. 19, nos. 1–4, pp. 9–20, 2000.

[12] E. G. Moody, M. D. King, C. B. Schaaf, and S. Platnick, "MODIS-derived spatially complete surface albedo products: Spatial and temporal pixel distribution and zonal averages," *J. Appl. Meteorol. Climatol.*, vol. 47, no. 11, pp. 2879–2894, 2008.

[13] G. Zibordi *et al.*, "Coastal atmosphere and sea time series (CoASTS), Part 1: A tower-based, long-term measurement program," NASA GSFC, Greenbelt, MD, USA, Tech. Rep. 2002-206892, 2002, vol. 19, pp. 1–29.

[14] C. Hu *et al.*, "Dynamic range and sensitivity requirements of satellite ocean color sensors: Learning from the past," *Appl. Opt.*, vol. 51, no. 25, pp. 6045–6062, 2012.

[15] G. Zibordi, F. Mélin, and J. F. Berthon, "Trends in the bias of primary satellite ocean-color products at a coastal site," *IEEE Geosci. Remote Sens. Lett.*, vol. 9, no. 6, pp. 1056–1060, Nov. 2012.